



Facile synthesis and characterization of pH-dependent pristine MgO nanostructures for visible light emission

Neeraj Marwaha¹, Bipin Kumar Gupta¹, Rajni Verma¹, and Avanish Kumar Srivastava^{1,*}

¹CSIR - National Physical Laboratory, Academy of Scientific and Innovative Research, Dr. K. S. Krishnan Marg, New Delhi 110012, India

Received: 30 March 2017

Accepted: 23 May 2017

Published online:

2 June 2017

© Springer Science+Business Media New York 2017

ABSTRACT

Herein, we demonstrate a strategy for facile synthesis of pristine MgO nanostructures at different pH values ranging from 7.9, 8.3 and 12.5 to explore their photoluminescence studies. These pH-dependent MgO nanostructures were characterized by various standard techniques such as XRD, SEM, EDS, TEM and photoluminescence (PL) spectroscopy. The obtained PL results clearly demonstrate that the PL emission spectra strongly depend upon growth environment. These nanostructures show a broad PL emission in visible region ranging from 400 to 680 nm at excitation wavelength of 330 nm. Hence, this study provides a unique feature to tailor the PL property of pristine MgO nanostructures which could be potentially used in luminescence harvesting for various optical display devices and sensing applications.

Introduction

Magnesium oxide (MgO) is one of the most important alkaline earth metal oxides due to its good optical property, wide band gap (7.8 eV), highly economical availability, low toxicity and eco-friendly nature [1, 2]. Recently, several studies have been focused on MgO nanostructures worldwide due to its fascinating morphologies like nanorods, nanospheres, nanoparticles, nanoflakes [3–9]. These fascinating nanostructures depend on the route of synthesis and different growth conditions. Although many efforts have been made to synthesize MgO nanostructures using various methods like sol-gel [10], thermal evaporation, combustion aerosol, chemical vapour deposition, hydrothermal [11] and

co-precipitation [12], hydrothermal method has been adopted mainly for its advantages to produce different morphologies at different experimental conditions. The optical properties of these nanostructures depend upon shape, size and various growth parameters which are directly related to the presence of intrinsic and extrinsic defects induced [13, 14]. Previous literature reports based on bare MgO nanostructures show intrinsic defects such as oxygen/magnesium ion vacancies (F-centre defects and V-centre defects) originate PL emission in the blue region at room temperature, while MgO with external defects (doped impurities), such as Cr, Fe, Mn or other transition metal ions doping, produces red emission [15–21]. It is interesting to note that proposed study promises a wide photoluminescence

Address correspondence to E-mail: aks@nplindia.org; avanish.aks555@gmail.com

emission from UV to visible emissions in undoped MgO nanostructures. Additionally, this study provides tailoring of photoluminescence intensity emission while varying the pH parameter.

In the present investigations, a facile synthesis method has been adopted for harvesting the luminescence from undoped nanostructures. Furthermore, we have thoroughly analysed the structural, microstructural and photoluminescence property of undoped MgO at various pH conditions. Moreover, we have discussed the growth mechanism of these nanostructures in basic medium which affect the photoluminescence property as well as nucleation of nanostructures. The highest PL emission intensity was observed at 465 nm upon 330 nm excitation wavelength for pH 12.5. These studies suggest that this precise method of synthesis with high photoluminescence property could be used in optical display device applications.

Experimental

Materials and methods

MgO nanostructures were prepared via facile hydrothermal route by just varying the pH parameter. Magnesium chloride hexahydrate [$\text{MgCl}_2 \cdot 6\text{H}_2\text{O}$] (98%, Thomas Baker) as a precursor and sodium hydroxide [NaOH] (>97%, Sigma Aldrich) was used to vary the pH parameter. Double distilled water was used during the entire synthesis process.

Initially, $\text{MgCl}_2 \cdot 6\text{H}_2\text{O}$ (5.3 g) was added to appropriate amount of deionized water (50 ml), say solution A. Then, 2 g of NaOH was mixed to 10 ml deionized water, say solution B. After that, the solution B was added dropwise to the solution A at 50 °C for 2 h to get white precipitate and adjust the pH values to 7.9, 8.3 and 12.5. The obtained white precipitate at different pH was put separately into autoclave at 250 °C for 10 h to get $\text{Mg}(\text{OH})_2$, and then as-synthesized $\text{Mg}(\text{OH})_2$ was further calcined at 500 °C/5 h to obtain MgO nanostructures.

Characterization

XRD experiments were carried out to obtain the crystalline structure, phase formation, purity and other information of synthesized MgO nanostructures using a Bruker X-ray diffractometer, with

monochromatic Cu $K\alpha_1$ radiation ($\lambda = 1.541 \text{ \AA}$) as a X-ray source in the scanning range from 10° to 80°. The morphological study of the nanostructures was carried out by scanning electron microscopy (Model: Zeiss EVO MA-10 SEM equipped). An energy-dispersive X-ray spectrum of MgO was executed by EDS: Oxford Link ISIS 300. Transmission electron microscopy (TEM) was performed for high-resolution morphology characterization, and HRTEM was used for the calculation of lattice spacing (HRTEM: FEI Tecnai G2 F30 STWIN at 300 kV). Photoluminescence characteristics were observed using a photoluminescence spectrometer (Edinburgh Instruments, model FLSP-900) with a xenon lamp as the excitation source.

Results and discussion

Phase identification

Figure 1 represents the XRD pattern of MgO nanostructures obtained at pH 12.5. All diffraction peaks located at $2\theta = 37.0^\circ, 43.0^\circ, 62.4^\circ, 74.9^\circ$ and 78.8° were well indexed and closely matched with cubic structure of MgO (JCPDF-ICDD card no. 87-0653).

There are no peaks corresponding to any impurity and signifying the completion of chemical reaction. Similarly, we have also observed the XRD patterns of MgO synthesized at 7.9 and 8.3. The peak centred at 43.0° with FWHM (obtained by Gauss fit to the

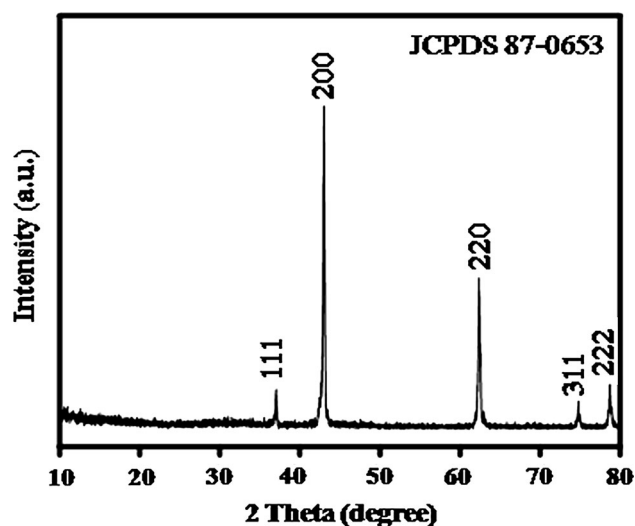


Figure 1 XRD graph of MgO nanostructures synthesized at pH 12.5.

relevant peak) 0.017 was used for the calculation of average crystallite size of MgO nanostructures synthesized at pH 12.5. The estimated average crystallite size by the Scherrer relation was 39 nm. The careful analysis reveals that the diffraction peak positions were identical but intensities of the peaks were decreased. FWHM values increase as the crystallite size decreases significantly from 39 to 25 nm with the variation in pH values to 7.9 from 12.5.

Micrograph investigation by SEM and TEM

The surface morphology and microstructural information of the synthesized MgO nanostructures have been investigated through SEM and TEM techniques.

Figure 2 represents the SEM micrographs of MgO nanostructures synthesized at different pH values of 7.9 and 8.3 at different magnifications. Micrographs project the evolution of different surface morphologies with varying pH values. At the lower pH of 7.9, non-uniform and spherical morphology can be observed as shown in Fig. 2a–b. As the pH was raised to 8.3, the flake-like morphology of the agglomerated nanostructures is noticed as depicted in Fig. 2c, d. At the higher pH of 12.5, uniform grain morphology with well-defined shape of agglomerated nanoparticles is noticed as represented in Fig. 3a–c. The range

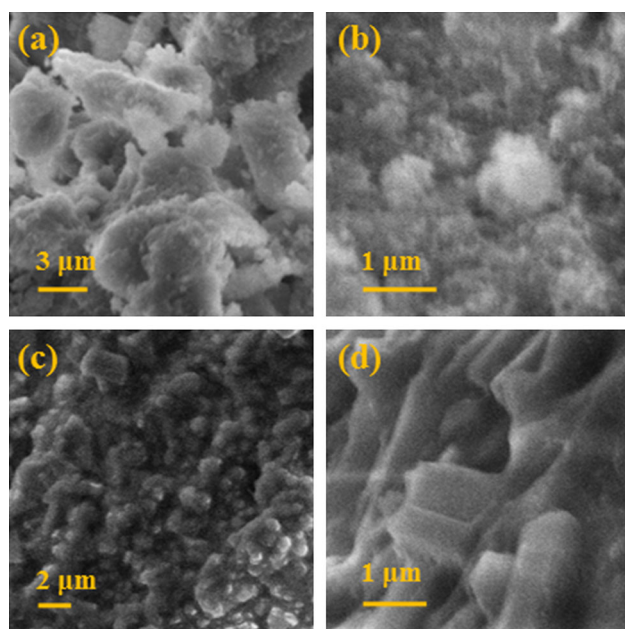


Figure 2 SEM micrographs of MgO nanostructures synthesized at different pH values at different magnifications; a, b pH 7.9 and c, d pH 8.3.

of particle size was found to be 0.3–0.6 μm as elucidated in Fig. 3c. The EDS analysis (Fig. 3d) of MgO nanostructures reveals the presence of Mg and O

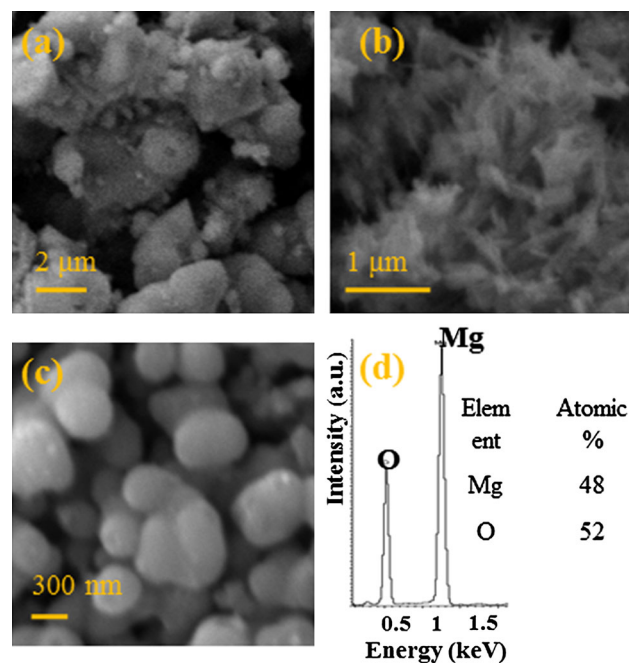


Figure 3 a–c SEM micrographs of MgO nanostructures at pH 12.5 at different magnifications, d corresponding EDS pattern.

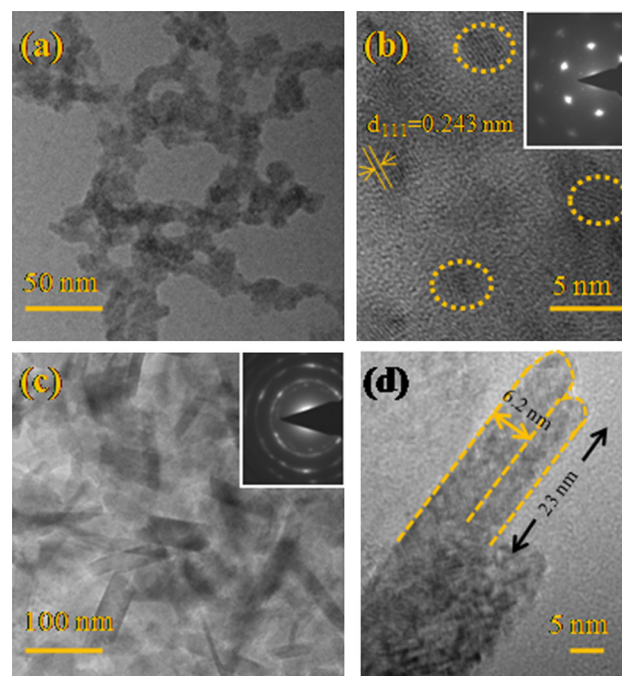


Figure 4 TEM micrographs of MgO nanostructures synthesized at a–b pH 7.9 and c–d pH 8.3. Insets in b and c represent SAED pattern.

atomic % of Mg/O to be 48:52. To scrutinize the exact size of the agglomerated particles at pH 12.5, HRTEM was performed.

Figures 4 and 5 demonstrate TEM of MgO nanostructures synthesized at different pH values. Figure 4a represents low-magnification MgO nanostructures obtained at pH 7.9. The micrograph depicts chain-like microstructures. The well-defined lattice fringes of d-spacing 0.24 nm correspond to [111] plane as elucidated in Fig. 4b. Inset in Fig. 4b represents bright spots that correspond to the higher crystallinity of obtained nanostructures. As the pH

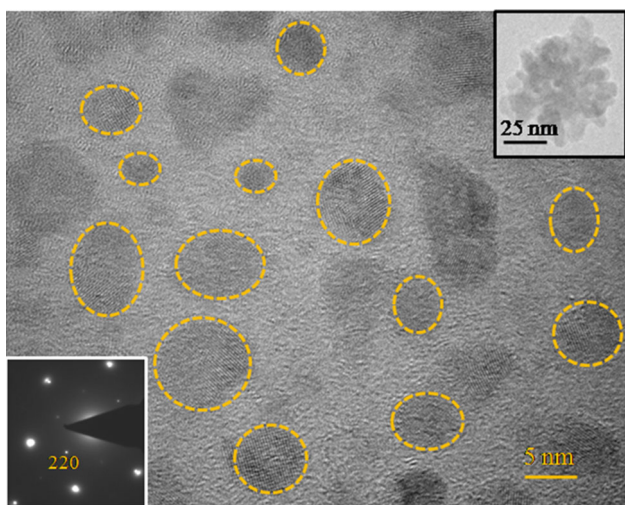


Figure 5 HRTEM image of MgO nanoparticles synthesized at pH 12.5. *Insets upper* show low-magnification image, *lower* shows SAED pattern.

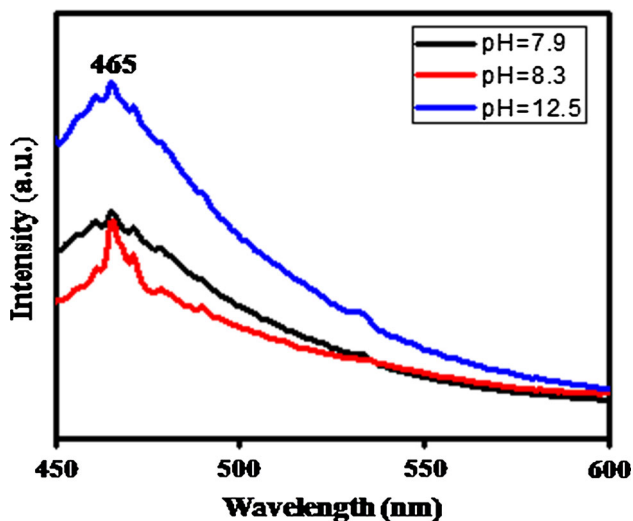


Figure 6 PL spectra of MgO nanostructures synthesized at various pH values.

was increased to 8.3, the nanoparticles turn into flake-like microstructure as represented in Fig. 4c. The inset in Fig. 4c represents the polycrystallinity of nanosized MgO. The width was ~ 6.2 nm, whereas the length was ~ 23 nm as shown in Fig. 4d.

Non-agglomerated particles can be observed as the pH was increased to 12.5 as shown in Fig. 5. The lower inset of Fig. 5 represents the electron diffraction pattern of MgO at pH 12.5.

Optical property evolution

Room-temperature photoluminescence spectra of MgO samples, synthesized at various pH values, were carried out at the excitation wavelength (λ_{ex}) of 330 nm as shown in Fig. 6. The emission spectrum depicts a peak at 465 nm (blue region) at the excitation wavelength of 330 nm. The emission at 465 nm corresponds to F-centre oxygen vacancies [1]. The PL results reveal that the emission intensity of MgO increases as pH values change from 7.9 to 12.5. At higher pH, the PL intensity increases due to higher spherical size leading to higher surface area. This may be because different growth conditions at different pH initiate the different rate of reaction for formation of the MgO nanostructures product. At higher pH (basic medium), co-nuclei effect results in the formation of larger nanoparticles as compared to that at lower pH. Therefore, PL intensity decreases at lower pH due to small particle size. Also, it is well established in the previous study that on increasing the temperature, particle size increases which leads to the increase in PL intensity [2]. Thus, the PL results provide a new route to tailor the intensity of the photoluminescence of MgO nanostructures by reducing a size-dependent technique.

Conclusions

In summary, MgO nanostructures have been synthesized by facile hydrothermal method by just varying the pH from 7.9 to 12.5, and then their photoluminescence studies were scrutinized. It was concluded that MgO nanostructures obtained at pH 12.5 show highest PL intensity peak at the excitation wavelength of 330 nm with emission of 465 nm. The PL results reveal that PL intensity increases with the increment in pH values. Because at higher pH (basic medium), several adjacent nuclei turn into co-nuclei

centres and result in the formation of larger nanoparticles as compared to that at lower pH which is also confirmed by HRTEM. Thus, this facile approach of change in pH parameter of MgO nanostructures provides the different PL intensity which could be potentially used in luminescence harvesting for various optical display devices applications.

Acknowledgements

We thank the Director, NPL New Delhi, India, for providing the necessary experimental facilities. Dr. Sushil Kumar, Dr. H. K Singh, Dr. Govind, Sh. Dinesh Singh and Sh. K. N. Sood are gratefully acknowledged for providing the necessary help and instrumentation facility for electron microscopy. The Project NanoSHE (BSC-0112) is gratefully acknowledged.

References

- [1] Roessler DM, Walker WC (1967) Electronic spectrum and ultraviolet optical properties of crystalline MgO. *Phys Rev* 159:733–738
- [2] Jain N, Marwaha N, Verma R, Gupta BK, Srivastava AK (2016) Facile synthesis of defect-induced highly luminescent pristine MgO nanostructures for promising solid-state lighting applications. *RSC Adv* 6:4960–4968
- [3] Suresh S (2014) Investigations on synthesis, structural and electrical properties of MgO nanoparticles by sol–gel method. *J Ovonic Res* 10:205–210
- [4] Florez E, Fuentealba P, Mondragon F (2008) Chemical reactivity of oxygen vacancies on the MgO surface: reactions with CO₂, NO₂ and metals. *Catal Today* 133:216–222
- [5] Vu AT, Jiang S, Kim YH, Lee CH (2014) Controlling the physical properties of magnesium oxide using a calcination method in aerogel synthesis: its application to enhanced sorption of a sulfur compound. *Ind Eng Chem Res* 53:13228–13235
- [6] Uchino T, Okutsu D, Katayama R, Sawai S (2009) Mechanism of stimulated optical emission from MgO microcrystals with color centers. *Phys Rev B Condens Mater Phys* 79:165107-1–165107-8
- [7] Shao C, Guan H, Liu Y (2006) MgO nanofibres via an electrospinning technique. *J Mater Sci* 41:3821–3824. doi:10.1007/s10853-005-5623-3
- [8] Taleshi F, Hosseini AA (2012) Synthesis of uniform MgO/CNT nanorods by precipitation method. *J Nanostruct Chem* 3:4
- [9] Mageshwari K, Sathyamoorthy R (2012) Studies on photocatalytic performance of MgO nanoparticles prepared by wet chemical method. *Trans Indian Inst Met* 65:49–55
- [10] Vinogradov AV, Vinogradov VV (2014) Low-temperature sol–gel synthesis of crystalline materials. *RSC Adv* 4:45903–45919
- [11] Cui H, Wu X, Chen Y, Boughton RI (2014) Synthesis and characterization of mesoporous MgO by template-free hydrothermal method. *Mater Res Bull* 50:307–311
- [12] Verma R, Naik KK, Gangwar J, Srivastava AK (2014) Morphology, mechanism and optical properties of nanometer-sized MgO synthesized via facile wet chemical method. *Mater Chem Phys* 148:1064–1070
- [13] Sternig A, Stankic S, Müller M, Bernardi J, Knozinger E, Diwald O (2008) Photoluminescent nanoparticle surfaces: the potential of alkaline earth oxides for optical applications. *Adv Mater* 20:4840–4844
- [14] Gangwar J, Gupta BK, Tripathi SK, Srivastava AK (2015) Phase dependent thermal and spectroscopic responses of different morphogenesis of Al₂O₃ nanostructures. *Nanoscale* 7:13313–13344
- [15] Stankic S, Bernardi J, Diwald O, Zinger EK (2006) How anesthetics, neurotransmitters, and antibiotics influence the relaxation processes in lipid membranes. *J Phys Chem B* 110:13858–13866
- [16] Remon A, Gagacia JA, Piqueras J (1986) Red luminescence from deformed MgO crystals. *J Phys Chem Solids* 47:577–580
- [17] Pikhitsa PV, Kim C, Chae S, Shin S, Jung S, Kitaura M, Kimura S, Fukui K, Choi M (2015) Two-band luminescence from an intrinsic defect in spherical and terraced MgO nanoparticles. *Appl Phys Lett* 106:183106
- [18] Vingurt D, Fuks D, Landau MV, Vidrubb R, Herskowitz M (2013) Grain boundaries at the surface of consolidated MgO nanocrystals and acid–base, functionality. *Phys Chem Chem Phys* 15:14783–14796
- [19] Ertekin E, Wagner LK, Grossman JC (2013) Point-defect optical transitions and thermal ionization energies from quantum Monte Carlo methods: application to the F-center defect in MgO. *Phys Rev B* 87:155210-1–155210-7
- [20] Gerson AR, Bredow T (1999) MgO (100) Surface relaxation and vacancy defects: a semi-empirical quantum-chemical study. *Phys Chem Chem Phys* 1:4889–4896
- [21] Yang H, Yang SH, Takahashi S, Maekawa S, Parkin SSP (2010) Extremely long quasiparticle spin lifetimes in superconducting aluminium using MgO tunnel spin injectors. *Nat Mater* 9:586–593